Title

Accumulated 3-phosphoglycerate in darkness is a primary starting substrate for stepwise photosynthetic induction process in cyanobacteria

Authors

Kenya Tanaka[1,2], Tomokazu Shirai[3,4], Mami Matsuda[4], Akihiko Kondo[1,3,4,5], Tomohisa Hasunuma[1,3,4,*]

Affiliations

1. Engineering Biology Research Center, Kobe University, 1-1 Rokkodai, Nada, Kobe 657-8501, Japan
2. Research Center for Solar Energy Chemistry, Graduate School of Engineering Science, Osaka University, Toyonaka, Osaka 560-8531, Japan
3. RIKEN Center for Sustainable Resource Science, 1-7-22 Suehiro-cho, Tsurumi-ku, Yokohama, Kanagawa 230-0045, Japan
4. Graduate School of Science, Innovation and Technology, Kobe University, 1-1 Rokkodai, Nada, Kobe 657-8501, Japan
5. Department of Chemical Science and Engineering, Graduate School of Engineering, Kobe University, 1-1 Rokkodai, Nada, Kobe 657-8501, Japan

*Corresponding author: Tomohisa Hasunuma

Email: hasunuma@port.kobe-u.ac.jp

Abstract

In photosynthetic organisms, a smooth metabolic transition from dark to light conditions is essential for efficient CO_2 fixation and growth. Dark-to-light transition leads to activation of the enzymes of the Calvin-Benson-Bassham (CBB) cycle and initiates CO_2 fixation metabolism using energy and redox equivalents provided by the photosynthetic electron transfer reaction. While many enzymatic mechanisms of the light activation of the CBB cycle have been clarified to date, the metabolic distribution and dynamics underlying the smooth start of photosynthetic metabolism remain unclear. Here, we show rapid (on a time scale of seconds) dynamics of changes in absolute metabolite concentration and ^{13}C tracer incorporation during photosynthetic induction (PI) in the cyanobacterium *Synechocystis* sp. PCC 6803. By combining these data, we were able to estimate time-resolved nonstationary dynamics of metabolic fluxes during PI. This novel metabolic analysis indicated that the initial step of PI consists of the reduction of 3-phosphoglycerate (3PG), a metabolite that accumulates in dark conditions; notably, this step occurs before subsequent generation of ribulose-1,5-bisphosphate (RuBP) and CO_2 fixation by ribulose-1,5-bisphosphate

carboxylase/oxygenase (Rubisco). *In vivo* oxygen evolution measurement in the presence of a CBB cycle inhibitor further confirmed that the accumulated 3PG is a major initial substrate for RuBP generation and functions as a key electron sink before the initiation of CO_2 fixation. Our results indicate a fundamental mechanism supporting the seamless activation of photosynthetic metabolism after dark-to-light transitions.

Main text

In leaves and isolated chloroplasts, there is known to be a delay between the onset of illumination and achieving a maximum rate of photosynthetic CO_2 fixation[1]. Since this photosynthetic induction (PI) process was suggested more than a century ago[2], the underlying mechanisms have been investigated intensively. Since the 1960s, the activation processes of many of the enzymes in the Calvin-Benson-Bassham (CBB) cycle have been studied[3], including those of glyceraldehyde 3-phosphate dehydrogenase (GAPDH), fructose-1,6-bisphosphatase (FBPase), sedoheptulose-1,7-bisphosphatase (SBPase), phosphoribulokinase (PRK), and ribulose-1,5-bisphosphate carboxylase/oxygenase (Rubisco). The activities of these enzymes and known to be altered by changes in cellular environmental properties such as redox state, energy charge, and ion concentration; these changes themselves reflect the effects of the photosynthetic electron transfer reaction[4-6]. Eventually, an overview of PI process in the leaves of land plants was developed, and can be summarized as follows: enzymes of RuBP regeneration pathways are activated in the first 1-2 min of illumination, followed by completion of slower Rubisco activation and stomatal opening within 7 to 10 min[7].

In addition to these enzymatic mechanisms, recent analyses performed using a theoretical photosynthetic model have predicted that maintaining the appropriate concentrations of CBB cycle intermediates is crucial for the initiation of CO_2 fixation[8]. In fact, experimental evidence in cyanobacteria has confirmed that the transfer of the carbon supply from a storage polymer (glycogen) to the CBB cycle affects photosynthetic efficiency[9,10].

However, details of the metabolic distribution and metabolic flux dynamics essential for efficient PI remain unknown. This shortcoming likely reflects the fact that the metabolic change during PI is poorly understood. Although transient changes in metabolite levels have been reported during PI in algae, in the chloroplasts of spinach protoplasts, and in wheat and maize leaves[11-15], we have yet to obtain systematic understanding of metabolite dynamics due to the lack of comprehensive and quantitative analyses. Instead, the metabolic dynamics and stability of the CBB cycle have been analyzed by computational modeling using random sampling of kinetic parameters instead of using known metabolome and flux distribution as a basis for model parameterization, given the lack of these analyses[16].

Among oxygenic photosynthetic organisms, cyanobacteria are the only prokaryote; notably, in this class of organisms, most metabolic reactions are performed in a shared space, the cytoplasm. Thus, it is not obvious that the metabolic dynamics of PI in cyanobacteria is similar to that in leaves and chloroplasts. On the other hand, cyanobacteria fix CO_2 via the CBB cycle like that used in higher plants, and these prokaryotes are regarded as the likely ancestor of the plant chloroplast[17]. Despite its importance for further understanding PI processes across photosynthetic organisms, cyanobacterial metabolic dynamics during PI has not (to our knowledge) been studied to date.

The ideal way to systematize complicated metabolic changes during PI is to estimate metabolic flux changes, which represent the integrated network responses of enzymes and metabolites. Analysis of metabolic fluxes provides useful information regarding topics such as pathway bottlenecks and network regulation in biological systems[18]. Although metabolic flux analysis (MFA) using an isotope tracer enables the mapping of intracellular carbon fluxes[19], the approach cannot be applied to a metabolically nonstationary state where metabolic fluxes and pool sizes are variable. On the other hand, previously developed dynamic MFA, which incorporates specialized statistical approaches, has permitted the estimation of long-term flux changes over the culture interval[20,21]. There has been (to our knowledge) no appropriate approach for the quantitative determination of metabolic flux change in short, metabolically transient states, including that of PI.

To estimate nonstationary metabolic flux changes, the following relationship was employed. The accumulation rate of a metabolite in a metabolic network is defined as the sum of all fluxes producing that metabolite minus the sum of all fluxes consuming that metabolite, as represented in following equation:

$$r_i(\mathrm{t}) = \sum_j \alpha_j x_j(t) - \sum_k \alpha_k x_k(t) \tag{1}$$

where $x_j(t)$ is the flux through reaction j, α_j is a stoichiometric coefficient, and $r_i(\mathrm{t})$ is the accumulation rate of metabolite i [22]. An example of three fluxes is illustrated in Fig. 1a. To obtain accumulation rates for estimation of the flux values, it is necessary to examine the absolute concentration change of metabolites with high time resolution. Namely, the metabolic flux during PI can be calculated by quantifying the change in metabolite concentration over highly time-resolved intervals immediate following light irradiation.

The time-resolved absolute quantification during PI in cyanobacteria has not been performed so far due to the technical difficulties of absolute quantification and rapid sampling. Here, by developing the integrated process shown in Fig. 1b, we successfully quantified absolute metabolite concentration change at second-scale intervals during PI in the cyanobacterium *Synechocystis* sp. PCC 6803 (*Synechocystis* hereafter). Additionally, to identify active metabolic pathways during PI, ^{13}C labelling dynamics after light irradiation start was analyzed (Fig. 1c). These accurate concentration and labelling dynamics allowed us to conduct short-time dynamic metabolic flux analysis (STD-MFA) and to estimate nonstationary flux change during PI. These analyses demonstrated a stepwise activation behavior that supports the smooth start of photosynthetic metabolism in *Synechocystis*.

Results

Absolute concentration changes in central carbon metabolic pathways during PI. Firstly, we sought to determine the absolute concentration dynamics of intermediate metabolites in central

energy metabolism during PI in *Synechocystis*. As light irradiation rapidly causes metabolic variation driven by increases in ATP and NADPH via the photosynthetic electron transfer reaction, rapid sampling and quenching of cellular metabolic activity are necessary for detecting metabolic changes during PI. A standardized procedure for intracellular metabolome quantification requires multiple analytical steps, including quenching of microbial metabolic activity, separation of microbial cells from growth medium, and extraction of intracellular metabolites, followed by mass spectrometric metabolite analysis. These multistep processes largely impede accurate estimation of the '*in vivo*' cellular metabolic state. Typically, metabolic activities are stopped rapidly by adding a quenching solution such as a cold methanol solution, followed by harvesting cells. However, metabolite leakage in the quenching solution is known to interfere with precise quantification of metabolite levels[23]. Although quick filtration usually is used for rapid cell sampling before quenching and extraction processes, the '*in vivo*' metabolic state may change a great deal due to variation in the light environment during the filtration process in the case of photosynthetic microorganisms. Furthermore, extraction yields of water-soluble metabolites depend on the extraction solvent, given that such metabolites may decompose during extraction processes[24]. The exact determination of metabolite concentrations also is hampered by ion suppression effects during mass spectrometric analysis[25].

To overcome these problems, in the present study, we employed a combination of two strategies. Firstly, to analyze intracellular metabolites, cells were separated from growth medium and suspended in 1 mM $NaHCO_3$ prior to metabolite sampling. This allowed quenching and extraction of intracellular metabolites merely by directly dropping the cell suspension into the extraction solution during light irradiation, and avoided metabolic state variation during the sampling process. We chose phenol-chloroform-isoamylalcohol (PCI) solution (pH 7.9) as an extraction solution because PCI extraction enabled rapid and efficient extraction of NADPH from *Synechocystis*[26]. Note that the exchange of medium for $NaHCO_3$ solution is a typical pretreatment for measuring photosynthetic activity of fresh-water cyanobacteria[27]. Secondly, stable isotopomers of the analyte compounds were used as an internal standard (IS). Although experimental protocols using the isotope-labeled IS have been developed for absolute quantification of metabolite concentration in various microorganisms including cyanobacteria[28-31], few attempts (to our knowledge) have been made to apply this accurate quantification method to time course analysis.

Figure 1b shows the experimental process for the exact determination of the absolute metabolite concentration dynamics of PI. We prepared a ^{13}C-labeled IS mixture by extracting metabolites from *Synechocystis* cells cultivated with $NaH^{13}CO_3$ as the sole carbon source. Absolute concentrations of uniformly ^{13}C-labeled metabolites were determined using capillary electrophoresis-mass spectrometry (CE-MS) based on the ratio between peak areas of known concentrations of unlabeled compounds included as an IS and the uniformly ^{13}C-labeled metabolites. Then, to quantify absolute concentration change during PI, dark-adapted *Synechocystis* cells (grown

149 in darkness for 12 h) were illuminated at a light intensity of 30 μmol m^{-2} s^{-1} (the same as the growth
150 light intensity) or 200 μmol m^{-2} s^{-1}. Metabolites of these cells were extracted rapidly using PCI
151 solvent containing the ^{13}C-labeled extract as a labeled IS whose concentration was determined using
152 another aliquot in the same extraction batch. Importantly, because of the high physicochemical
153 similarities between the labeled IS and the unlabeled analyte, the two mixtures undergo similar
154 opportunities for degradation and ion suppression effects, permitting compensation for the above
155 drawbacks[28-31]. Given that the absolute metabolite concentrations were determined based on the ratio
156 between unlabeled and uniformly labeled peak areas (Fig. 1b), the process was expected to prevent
157 contamination of unlabeled metabolites in the ^{13}C-labeled IS. The proportions of uniformly
158 ^{13}C-labeled metabolites (compared to sum of unlabeled and uniformly labeled metabolites) were
159 found to exceed 95% for all metabolites except for citrate (Supplementary Fig. 1). Figure 2 shows
160 the temporal change of the absolute metabolite concentration after the initiation of light irradiation at
161 30 μmol m^{-2} s^{-1} or 200 μmol m^{-2} s^{-1}. It should be noted that a small amount of some metabolites
162 was extracellular (Supplementary Fig. 2). A previous study that measured NADPH fluorescence *in*
163 *vivo* revealed that the amount of NADPH in *Synechocystis* increased within 0.5 s of illumination[32].
164 The rapid increase of NADPH observed within 5 s in the present work was consistent with that
165 earlier *in vivo* study, confirming that this metabolomics analysis successfully detected the rapid start
166 of photosynthesis. As with NADPH, the level of the energy cofactor ATP also was observed to
167 increase rapidly. Overall, the levels of 3-phosphoglycerate (3PG), 2-phosphoglycerate (2PG), and
168 phosphoenolpyruvate (PEP) decreased; the levels of other CBB cycle intermediates (excepting 3PG,
169 ribulose 5-phosphate (Ru5P) and xylulose 5-phosphate (Xu5P)) increased, while the levels of
170 tricarboxylic acid (TCA) cycle intermediates did not change appreciably. Considering these
171 metabolite variations together, we inferred that accumulated glycolysis intermediates including 3PG,
172 2PG, and PEP likely were converted to CBB cycle intermediates at the initial step of PI.
173
174 **^{13}C labeling kinetics during PI**. A direct way to confirm this hypothesis is to determine the
175 metabolic flux distribution at PI. However, the precise metabolic flux values cannot be determined
176 when the number of unknown flux parameters is larger than that of known metabolite concentration
177 changes in a metabolic model system used for flux calculation. To perform STD-MFA, we sought to
178 refine the metabolic model by excluding metabolic pathways that are inactive during PI. However,
179 the metabolite concentration data in Fig. 2 cannot identify the inactive metabolic pathways. Notably,
180 even if the metabolic concentration change is zero, metabolic flux is not necessarily zero, because
181 such an observation instead may indicate that metabolic inflow and outflow are balanced. In the case
182 where the concentration of a metabolite is stable and ^{13}C is not incorporated into the metabolite
183 during photosynthetic $^{13}CO_2$ fixation, the metabolic fluxes around the metabolite are estimated to be
184 very small, and so can be neglected. Therefore, we next measured the dynamics of ^{13}C isotope

incorporation after the transition from dark to light conditions by starting photosynthesis while the cells were suspended in a solution of $NaH^{13}CO_3$. Figure 3 shows time courses of transient changes in the atomic fraction of labeled carbon. In contrast to the high ^{13}C fraction seen for CBB cycle intermediates, 6-phosphogluconate (6PG) and TCA cycle intermediates (except for malate and fumarate) were not labeled. In addition, the ^{13}C fraction of ADP-glucose, which is known to be a precursor of glycogen[33], was low. When these results were considered together with those indicating that the concentrations of these metabolites did not change appreciably during PI (Fig. 2), we inferred that the metabolic fluxes in the TCA cycle, the oxidative pentose phosphate pathway (OPPP), the Entner-Doudoroff pathway (EDP), and the glycogen synthesis pathway are extremely low immediately after light irradiation.

Other than Rubisco, the primary metabolic enzymes that incorporate CO_2 are phosphoenolpyruvate carboxylase (PepC) and malic enzyme (ME), which are directly or indirectly connected to malate (Fig. 3). Since malate was not labelled until 60 s after the initiation of light irradiation (at both of the tested light intensities), ^{13}C incorporation before 60 s was inferred to reflect Rubisco activity. The amount of incorporated ^{13}C atom was calculated by multiplying the measured ^{13}C fraction (shown in Fig. 3) by the absolute carbon concentration of each metabolite (shown in Fig. 2); these analyses are presented in Extended Data Fig. 1 a and b. The total amount of incorporated ^{13}C atom was derived by summing the number of ^{13}C atoms of all measured metabolites (Extended Data Fig. 1c, d). Notably, ^{13}C incorporation did not start until 12 s after the initiation of light irradiation. On the other hand, ^{13}C incorporation was observed at least 10 s after the addition of $NaH^{13}CO_3$ to cells whose photosynthetic activity already had been activated by 5 min of illumination (Extended Data Fig. 2). Together, these results suggested that the observed delay in the start of ^{13}C incorporation (compared to the start of light irradiation) was not attributable to slow uptake of $NaH^{13}CO_3$ by the cells. Instead, these data indicated that the fixation of CO_2 through Rubisco remains inactive at the initial stage of photosynthetic metabolism (i.e., immediately following the start of illumination). Although the delayed onset of CO_2 fixation is a well-known phenomenon in plant leaves[1], this observation in the present work is (to our knowledge) the first direct demonstration of a Rubisco activation effect in the *in vivo* metabolic dynamics in cyanobacteria.

It is interesting to note that labeled carbon was incorporated into malate and fumarate after 120 s, particularly in cells illuminated at 200 μmol m^{-2} s^{-1}, at a time when other TCA cycle intermediates remained unlabeled. This result suggested that malate and fumarate are generated by the reductive TCA pathway, which is known as a fermentation pathway employed for NADH oxidation[34]. Thus, the accumulation of NADH may drive the activity of this reductive TCA pathway (Extended Data Fig. 3).

Short-term dynamic metabolic flux analysis (STD-MFA). Finally, we calculated temporal changes in the net metabolic fluxes based on the obtained data. As mentioned above, during the first 60 s of illumination, the net metabolic fluxes in pathways other than the CBB cycle and glycolysis until 60 s appeared to be very small. In fact, the concentrations of newly synthesized (labeled) amino acids before 60 s were hardly changed, even in cells illuminated at 200 μmol m^{-2} s^{-1}, although the labeled levels of some amino acids (serine, alanine, phenylalanine, tyrosine and ornithine) increased significantly after the first minute of illumination (Extended Data Fig. 4). Furthermore, photorespiratory intermediates such as glycolate, glyoxylate, and glycerate did not accumulate during the first 60 s of illumination (Extended Data Fig. 5). Therefore, we assessed the metabolic pathways shown in Extended Data Fig. 6a as part of the subsequent calculations, focusing on metabolic dynamics during the first 60 s following the initiation of illumination.

To solve equation (1) and conduct STD-MFA, accumulation rates for metabolites in the metabolic model shown in Extended Data Fig. 6a were derived from the slopes obtained between two consecutive concentration data points in Fig. 2. In addition to our use of equation (1), we calculated the CO_2 fixation rate as the increase in the rate of total ^{13}C incorporation (Extended Data Fig. 1). Specifically, the latter parameter was interpreted as the metabolic flux from RuBP to 3PG, given that the ^{13}C incorporation experiment mentioned above indicated that all carbon atoms fixed during the first 60 s of illumination were attributable to Rubisco activity. The net metabolic fluxes of each time interval were estimated by solving these equations simultaneously (Fig. 4, Extended Data Fig. 6). The estimated flux values were validated and judged to be reliable, given that almost all of the estimated metabolite accumulation rate values (which were derived from the estimated fluxes) yielded values that were within the mean ± SD range of the measured accumulated rate (Extended Data Fig. 7). For more details of the calculation process and equations, see the Methods section.

The time course of flux distribution clearly indicated that photosynthetic metabolism in *Synechocystis* starts in a stepwise manner: first, activation of the reduction of 3PG to glyceraldehyde 3-phosphate (GAP); second, generation of RuBP; and third, Rubisco activation (Fig. 4, Extended Data Fig. 6c, d). Interestingly, the induction of RuBP generation can be further divided into two sub-steps based on metabolic fluxes, given that the formation fluxes of C6 intermediates (fructose 1,6-bisphosphate (FBP) and fructose 6-phosphate (F6P)) increased faster than that of C7 intermediates (sedoheptulose 1,7-bisphoshate (SBP) and sedoheptulose 7-phosphate (S7P)) (Extended Data Fig. 6c,d). Notably, the C6 and C7 pathways share an enzyme, fructose-1,6-bisphosphatase, in common, which (in *Synechocystis*) is known to be a bi-functional fructose-1,6-/sedoheptulose-1,7-bisphosphatase (FBP/SBPase)[35]. Thus, modification of enzymatic activity is unlikely to be the cause of the activation time gap between the two pathways. In the CBB cycle, the production of erythrose 4-phosphate (E4P), a starting substrate of the C7 pathway, depends on the activity of the C6 pathway. Therefore, we inferred that substrate deficiency in the C7

257 pathway is attributable to the metabolic pathway topology in the CBB cycle, delaying the C7
258 pathway relative to the C6 pathway in *Synechocystis*.
259 The reduction fluxes of 3PG differed greatly between cells illuminated at 30 and 200 μmol
260 m^{-2} s^{-1}, even before the initiation of CO_2 fixation (i.e., during the first 5-20 s) (Fig. 4). In
261 steady-state photosynthesis, the increased rate of electron donor (NADPH) production from the
262 photosynthetic electron transfer reaction at the higher light intensities becomes balanced with the
263 rate of electron acceptor (3PG) production that also is increased by elevated CO_2 fixation rate. On
264 the other hand, before the onset of CO_2 fixation immediately following the initiation of light
265 irradiation, excess reducing power can be accumulated because 3PG cannot be produced while
266 NADPH is produced by the electron transfer reaction. Nevertheless, the increase in the reducing
267 fluxes of 3PG with the higher light intensity (200 μmol m^{-2} s^{-1}) before CO_2 fixation suggests that
268 even before the onset of CO_2 fixation, the rate of 3PG consumption is balanced with the rate of
269 NADPH production rate from the electron transfer reaction, which varies with light intensities. In
270 addition, it clearly can be seen that 2PG and PEP were converted to 3PG at the both light intensities
271 (Fig. 4). Therefore, we proposed that accumulation of these glycolytic intermediates provides a
272 "stand-by" state and flexibility for the initiation of photosynthetic metabolism before the start of CO_2
273 fixation; thus, these intermediates are expected to play an important role in balancing cofactor
274 regeneration and consumption during PI.
275
276 **Oxygen evolution in the presence of a CBB cycle inhibitor.** To confirm the function of 3PG as an
277 electron acceptor at the start of photosynthesis *in vivo*, we measured the oxygen evolution rate in the
278 presence of a CBB cycle inhibitor, glycolaldehyde (GA). GA is known to inhibit the conversion of
279 triose phosphate to RuBP in the CBB cycle, thereby impeding oxygen evolution during steady-state
280 photosynthesis in cyanobacteria[36]. If 3PG is serving as an electron acceptor for NADPH generated
281 by the photosynthetic electron transfer reaction, oxygen evolution in light-exposed, GA-treated cells
282 should proceed only until the accumulated 3PG is exhausted. As expected, GA-treated cells
283 generated oxygen starting just after the initiation of illumination, but oxygen evolution by these cells
284 diminished rapidly after 25 s of irradiation with 200 μmol m^{-2} s^{-1} light (Fig. 5a). Based on
285 theoretical stoichiometry, two molecules of NADPH produced by one molecule of oxygen evolution
286 reduce two molecules of 3PG. The total decreasing rate of 3PG, 2PG and PEP immediately after 200
287 μmol m^{-2} s^{-1} light irradiation was about twice that of oxygen evolution rate in GA-treated cells (Fig.
288 5a, c). This quantitatively supports that the accumulated glycolytic metabolites acted as electron
289 acceptors for oxygen evolution in GA-treated cells. Moreover, the oxygen evolution rate of
290 GA-treated cells from the onset of the 200 μmol m^{-2} s^{-1} illumination to 25 s was identical to the
291 oxygen evolution rate of non-treated cells (Fig. 5a). This suggests that even in a normal PI process of
292 non-GA-treated cells, the electron acceptors that contributes to the initial oxygen evolution in PI are

293 the accumulated glycolytic intermediates. In cells irradiated with 30 μmol m^{-2} s^{-1} light irradiation,
294 no significant difference in oxygen evolution rate dynamics was observed between GA-treated and
295 non-treated cells; this effect presumably reflected slow consumption and depletion of 3PG in
296 GA-treated cells (Fig. 5b, d). In further confirmation of our hypothesis, we demonstrated depletion
297 of 3PG and inhibition of RuBP accumulation in GA-treated cells following irradiation with 200
298 μmol m^{-2} s^{-1} light (Extended Data Fig. 8). These results clearly indicated that accumulated 3PG
299 functions as a first electron acceptor for the rapid initiation of photosynthetic metabolism upon
300 exposure of dark-adapted cyanobacteria to light.
301
302 **Discussion**
303 In the present study, combined analysis of absolute metabolite concentrations and isotope
304 incorporation transients of a wide spectrum of metabolites permitted us to visualize changes in
305 nonstationary metabolic fluxes during PI in *Synechosystis*. The activation order during PI in
306 *Synechosystis* was found to be resemble that in land plants, where the activation of RuBP generation
307 typically precedes the start of CO_2 fixation[7]. However, the detailed order of activation of the various
308 pathways in plant leaves has not (to our knowledge) been investigated. STD-MFA revealed that the
309 step of activation of RuBP generation in *Synechosystis* involves two phases, the fast C6 pathway and
310 the slower C7 pathway. This distinction in timing was inferred to reflect the metabolic pathway
311 topology inherent to the CBB cycle. Furthermore, 3PG accumulated in the dark period was found to
312 be depleted rapidly, apparently functioning as a starting substrate for RuBP generation before the
313 start of CO_2 fixation. This rapid depletion of phosphoglycerate upon illumination also has been
314 observed in algae, in the chloroplast of spinach protoplasts, and in the leaves of a C3 plant
315 (wheat)[11,12,15]. In contrast, monotonic accumulation of phosphoglycerate has been reported in the
316 leaves of a C4 plant (*Zea mays*)[13,14]. We suspect that the difference in phosphoglycerate dynamics
317 during PI may reflect divergence between C3 and C4 photosynthetic metabolism, but clearly further
318 investigation is necessary.
319 A closer look at Fig. 2 permits a more detailed characterization of the details of the
320 individual metabolic pathways. Although increases in the levels of NADPH and ATP (which occur
321 within 5 s of the start of illumination) should make the reduction of 3PG to GAP energetically
322 favorable, a large decrease in the level of 3PG is observed after the 5-s time point. Cyanobacterial
323 phosphoglycerate kinase (PGK) and GAPDH are activated by reductive dissociation of cysteine
324 pairs upon light illumination[37,38]. Thus, the delay in 3PG consumption until after 5 s of illumination
325 likely is due to the need for the redox activation of PGK and GAPDH. Transient accumulation of
326 FBP indicates the existence of an activation period for the FBP/SBPase enzyme. FBP/SBPase in
327 *Synechocystis* is activated by reduction of a thiol group and binding of Mg^{2+}, and this enzyme is
328 inhibited allosterically by the binding of AMP[39,40]. Indeed, a rapid decrease of AMP concentration

329 was confirmed after light irradiation (Extended Data Fig. 3). In addition, temporal accumulation of
330 dihydroxyacetonephosphate (DHAP) upon irradiation with 200 μmol m^{-2} s^{-1} light may be
331 attributable to the transient rate-limitation of FBP/SBPase. The significantly higher continuous
332 accumulation of F6P and S7P in cells illuminated at 200 μmol m^{-2} s^{-1} (compared to those
333 illuminated at 30 μmol m^{-2} s^{-1}) indicates that the reaction catalyzed by the transketolase enzyme is
334 the major rate-limiting step. This interpretation is consistent with the results of a previous study,
335 which reported enhanced photosynthetic activity in a *Synechocystis* strain engineered to overproduce
336 transketolase[41]. Regarding RuBP dynamics, *Synechocystis* (like plants) requires Rubisco activation
337 processes, although the mechanism of this activation differs slightly between these two classes of
338 organisms[42]. Thus, the accumulation and subsequent decrease of RuBP in cyanobacteria suggests a
339 phase shift from inactivated to activated Rubisco. Indeed, similar dynamics of the RuBP pool size
340 was observed during PI in plant leaves, and is associated with Rubisco activation[43,44]. The levels of
341 GAP, E4P, and ribose 5-phosphate (R5P) were below the detection limit, suggesting that these
342 metabolites are consumed rapidly and are not accumulated during PI. The levels of 2PG and PEP
343 decreased more slowly than those of 3PG. Phosphoglycerate mutase catalyzes the reversible
344 conversion between 3PG and 2PG, while enolase catalyzes the reversible conversion between 2PG
345 and PEP. To assess the direction of these processes, the reaction Gibbs energy change ($\Delta_r G$) of these
346 reactions was calculated based on following equation:

347 $$\Delta_r G = \Delta_r G^{\circ} + RT \ln Q \quad (2)$$

348 $$Q_{3PG \to 2PG} = \frac{[2PG]}{[3PG]}, Q_{2PG \to PEP} = \frac{[PEP]}{[2PG]}$$

349 where $\Delta_r G^{o}$ is the standard reaction Gibbs energy change, R is the ideal gas constant, T is the
350 temperature, and Q is the reaction quotient. As the conversions among 3PG, 2PG, and PEP are
351 simple reactions, where one reactant species is converted to one product (along with water),
352 consideration of cell volume is not necessary, allowing relatively precise estimation of $\Delta_r G$.
353 Therefore, we focused on the $\Delta_r G$ estimation of these reactions. Corresponding $\Delta_r G^{o}$ values were
354 obtained as the means of the experimentally determined values summarized in Bennett et al.[29]. The
355 changes in reaction Gibbs energy from 3PG to 2PG and from 2PG to PEP during the first 60 s of
356 light irradiation were positive values or approximately 0 (Extended Data Fig. 9). These analyses are
357 consistent with our inference that the direction of net metabolic flux is from PEP to 3PG
358 immediately following the initiation of light irradiation, as shown in Fig. 4.

359 Let us consider the mechanisms by which large amounts of 3PG are accumulated in
360 dark-adapted *Synechocystis*. Cyanobacteria utilize glycogen stored during the day for respiratory
361 metabolism at night. In mutant strains deficient in the synthesis or degradation of glycogen, the
362 activation of photosynthetic metabolism is delayed due to lack of CBB cycle intermediates[9,10]. On
363 the other hand, the enzymatic activities of the TCA cycle in *Synechocystis* are known to be lower

364 than those in other organisms[45]. Thus, we infer that the generation of glycolytic intermediates by
365 glycogen degradation and slow catabolic activity via TCA cycle are likely to cause the accumulation
366 of 3PG along with 2PG and PEP in dark-adapted *Synechocystis*.

367 The STD-MFA technique developed in this study is a method for quantifying changes over
368 time of metabolic flux during a dynamic phenomenon that induces rapid metabolic changes that
369 occur over short intervals (within a few minutes). This method requires measurement of
370 time-resolved absolute concentration changes and metabolic model refinement based on isotope
371 incorporation data before flux calculation. Previously developed dynamic metabolic flux analysis
372 methods typically are intended to estimate flux change over long periods of culture processes, and
373 require technically specialized mathematical approaches[20,21]. In contrast, STD-MFA permits the
374 direct determination of metabolic flux changes in exchange, albeit while focusing on short time
375 intervals. We expect that this method also may be of use for understanding other non-stationary rapid
376 metabolic changes that have been the recent focus of attention, such as the end of photosynthesis and
377 adaptation against oxidative stress[46,47].

378 We have demonstrated that the accumulation of glycolysis intermediates helps smooth
379 metabolic start of CBB cycle in *Synechocystis*. The rational metabolic engineering based on the
380 findings in this study may improve CO_2 fixation rate and growth of synthetic autotrophic
381 microorganisms, which need further metabolic optimization[48,49]. This will lead to construction of
382 efficient bio-based chemical production from CO_2.

383

384 **Methods**

385 **Growth conditions**

386 This work employed a glucose-tolerant wild strain of *Synechocystis*[50] that was grown and stored on
387 solid BG-11 media plates (containing 1.5% Bacto agar). Pre-culturing was performed in 200-mL
388 flasks containing 50 mL each of liquid BG-11 medium buffered with 20 mM
389 2-[4-(2-hydroxyethyl)-1-piperazinyl]ethanesulfonic acid (HEPES, pH 7.5); each flask was
390 inoculated with cells from the agar plates. These flasks then were cultured at 30 ºC in ambient air
391 with shaking at 100 rpm; illumination at an intensity of 30 μmol $m^{-2}s^{-1}$ was provided by white
392 light-emitting diode (LED) lights. The main culture was initiated by adding pre-culture grown for 4
393 days into a 70-mL quantity of the BG-11 medium to give an optical density of 0.05 at 730 nm
394 (OD_{730}). The growth condition of the main culture was the same as that of the pre-culture. The dry
395 cell weight (DCW) was measured after harvesting cells by centrifugation and lyophilization. The
396 obtained relationship between OD_{730} value and DCW ($DCW = 0.1998 \times OD_{730} \times V + 0.0974$;
397 R^2=0.982; n=9; V is volume of cell suspension) was used for estimating DCW from the OD_{730} value.

398

399 **Preparation of ^{13}C isotope-labeled internal standard (^{13}C-IS)**

400 *Synechocystis* cells in pre-culture were inoculated to an OD_{730} of 0.05 in a serum bottle containing
401 60 mL modified BG-11 medium supplemented with 100 mM HEPES (pH 7.5) and 25 mM
402 $NaH^{13}CO_3$ (in place of the unlabeled Na_2CO_3 included in the standard BG-11 medium). The culture
403 serum bottle was sealed, followed by flushing with N_2 gas to remove unlabeled ambient CO_2. The
404 growth condition of the labeled culture was the same as that of the pre-culture and main culture.
405 Cells grown for 3 days were harvested and re-suspended in fresh modified BG-11 to avoid pH
406 increase during cultivation with $NaH^{13}CO_3$ as the sole carbon source. The labeled culture then was
407 grown under the same conditions for another 3 days, followed by extraction of uniformly labeled
408 metabolites as described below.
409 The entire volume of the labeled culture was harvested by centrifugation, washed with 1 mM
410 $NaH^{13}CO_3$ solution, and then re-suspended in 9 mL of 1 mM $NaH^{13}CO_3$. The resulting cell
411 suspension was illuminated for 90 s with white LED light at an intensity of 200 μmol $m^{-2}s^{-1}$ (to
412 maximize extraction yield of CBB cycle intermediates), and dropped into a mixture of 9 mL PCI (pH
413 7.9, Nacalai tesque, Kyoto, Japan) and 60 μL 0.5 M N-cyclohexyl-3-aminopropanesulfonic acid
414 (CAPS, pH 10.6) for metabolite extraction. The extraction mixture was centrifuged at 4 ºC at 8,000
415 ×g for 3 min. Twelve to 13 fractions of the water layer were aliquoted into microtubes and
416 lyophilized.
417 One of the dried aliquots was dissolved in 20 μL of standard mixture containing prepared unlabeled
418 compounds. The sample was analyzed by capillary electrophoresis-mass spectrometry (CE-MS) (CE,
419 Agilent G7100; MS, Agilent G6224AA LC/MSD TOF; Agilent Technologies, Palo Alto, CA, USA)
420 as described previously[51]. Absolute concentrations of the uniformly labeled isotopomer (C_n) were
421 derived as follows:

422 $$C_n = \frac{S_n}{S_0} C_0 \quad (3)$$

423 where S_n and S_0 are peak areas of uniformly ^{13}C-labeled (namely, the number of ^{13}C atoms in a
424 n-carbon compound is equal to n) and unlabeled standard signals, respectively, and C_0 is the
425 prepared concentration of the unlabeled standard.
426
427 **Metabolite extraction with rapid sampling and analysis**
428 To perform metabolite sampling for analyses of absolute concentration and ^{13}C incorporation after
429 transition from dark to light, a main culture grown for 6 days was dark-adapted for 12 h. A calculated
430 volume (90/OD_{730}, in mL) of the dark-adapted cell culture was harvested by centrifugation at
431 8000×g for 5 min. The cells were washed with 4 mL of 1 mM $NaHCO_3$ (for absolute concentration
432 analysis) or 1 mM $NaH^{13}CO_3$ (for ^{13}C incorporation analysis), and harvested again by centrifugation.
433 The washed cells were resuspended in 6.8 mL of 1 mM $NaHCO_3$ (for absolute concentration
434 analysis) or 1 mM $NaH^{13}CO_3$ (for ^{13}C incorporation analysis). Nine aliquots (750 μL each) of the

resulting cell suspension were loaded into clear pipet tips (Supplementary Fig. 3). Up to this point, light irradiation was avoided during the procedure to keep the cells in the dark-adapted state. Irradiation of all the aliquots with white LED light at an intensity of 200±10 μmol $m^{-2}s^{-1}$ or 30±2 μmol $m^{-2}s^{-1}$ was initiated, followed by sampling of the cells at the indicated time points by dropping into 750 μL PCI supplemented with ^{13}C-IS dissolved in 20 μL water (for absolute concentration analysis) or with 5 μL of 0.5 M CAPS (pH 10.6) (for ^{13}C incorporation analysis). The cell suspension before illumination was extracted as the nominal 0-s sample. To precisely determine the amount of extracted cells, the OD_{730} of the final cell suspension was measured. After the extraction mixtures were centrifuged at 4 ºC at 12,000×g for 2 min, harvested aliquots of the water layer were lyophilized.

The lyophilized samples were dissolved in 20 μL of 0.4 mM piperazine-1,4-bis(2-ethanesulfonic acid) (PIPES) and analyzed by CE-MS as described above. Absolute concentrations of each metabolite (*C'*) were derived as follows:

$$C' = \frac{S'_0}{WS'_n} C_n V \tag{4}$$

where S'_0 and S'_n are peak areas of unlabeled and uniformly ^{13}C-labeled IS signals, respectively, W represents DCW, and V is sample volume for CE-MS analysis. ^{13}C fractions were calculated as described previously[34].

Short-term dynamic metabolic flux analysis (STD-MFA)

To estimate temporal changes of 18 fluxes in the metabolic map shown in Extended Data Fig. 6, eighteen metabolite accumulation rates r_i(t) in equation (1) were derived from the slope taken between two consecutive concentration data points shown in Fig. 2. Accumulation rates of metabolites under the detection limit (E4P, R5P, GAP < 0.001 nmol/mg DCW) and peak-unidentified metabolites (BPG and SBP) were set to zero. In addition, the CO_2 fixation rate derived from the slope taken between two consecutive data points shown in Extended Data Fig. 1c and d was regarded as the metabolic flux of Rubisco (i.e., the conversion of RuBP to 3PG). The set of 19 equations, including the 18 unknown fluxes in the network, was represented in matrix notation as follows:

$$\mathbf{A}\mathbf{x}(\mathrm{t}) = \mathbf{r}(t) \tag{5}$$

where A was the 19 × 18 matrix of stoichiometric coefficients, **x**(t) was the 18-dimensional flux vector, and r(t) was the 19-dimensional metabolite accumulation rate vector. The specific form of equation (4) is shown in Extended Data Fig. 6b. The weighted least squares solution to equation (5) is as follows:

$$\hat{\mathbf{x}}(\mathrm{t}) = (\mathbf{A}^T\mathbf{W}\mathbf{A})^{-1}\mathbf{A}^T\mathbf{W}\bar{\mathbf{r}}(t) \tag{6}$$

where the superscripts ^ and ¯ denote estimated and measured quantities (respectively), and **W** is

a 19-dimensional weighting diagonal matrix, whose diagonal elements are the reciprocal of the variance of the measured metabolic accumulation rate values. Variance values for the accumulation rate of E4P, R5P, GAP, BPG, and SBP, and for the CO_2 fixation rate, were set to 10^{-15} (i.e., a value that was effectively zero). To evaluate the reliability of the estimated fluxes, metabolite accumulation rates were calculated as follows:

$$\mathbf{A}\hat{\mathbf{x}}(t) = \hat{\mathbf{r}}(t) \tag{7}$$

The estimated and measured metabolite accumulation rate values are compared in Extended Data Fig. 7.

Oxygen evolution measurement

Synechocystis wild-type cells were collected and re-suspended in the same way as the preparation process in the metabolite sampling experiment described above. Whole-cell oxygen evolution was measured with light illumination at the intensity of 200 μmol $m^{-2}s^{-1}$ or 30 μmol $m^{-2}s^{-1}$ in a Clark-type oxygen electrode (Hansatech Instruments) containing 750 μL of the cell suspension.

References

1. Walker, D. A. Photosynthetic induction phenomena and the light activation of ribulose diphosphate carboxylase. *New Phytol.* **72**, 209–235 (1973).
2. Osterhout, W. J. & Haas, A. R. Dynamical Aspects of Photosynthesis. *Proc. Natl. Acad. Sci. USA.* **4**, 85-91 (1918).
3. Buchanan, B. B. Role of light in the regulation of chloroplast enzymes. *Ann. Rev. Plant Physiol.* **31**, 341-374 (1980).
4. Lorimer, G. H., Badger, M. R. & Andrews, T. J. The Activation of Ribulose-1,5,-bisphosphate carboxylase by carbon dioxide and magnesium ions. Equilibria, kinetics, a suggested mechanisms, and physiological implications. *Biochem*. **15**, 529-536 (1976).
5. Portis, Jr. A. R. The regulation of Rubisco by Rubisco activase. *J. Exp. Bot.* **46**, 1285-1291 (1995).
6. Michelet, L. et al. Redox regulation of the Calvin-Benson cycle: something old, something new. *Front Plant Sci* **4**, 470 (2013).
7. Pearcy, R. W., Krall, J. P. & Sassenrath-Cole, G. F. Photosynthesis in Fluctuating Light Environments. In: Baker NR, ed. *Photosynthesis and the Environment.* Dordrecht: Kluwer, 321–346 (1996).
8. Matuszyńska, A., Saadat, N. P. & Ebenhöh, O. Balancing energy supply during photosynthesis - a theoretical perspective. *Physiol. Plant* **166**, 392-402 (2019).
9. Shimakawa, G. et al. Respiration accumulates Calvin cycle intermediates for the rapid start

of photosynthesis in Synechocystis sp. PCC 6803. *Biosci. Biotechnol. Biochem.* **78**, 1997-2007 (2014).

10. Shinde, S. et al. Glycogen Metabolism Supports Photosynthesis Start through the Oxidative Pentose Phosphate Pathway in Cyanobacteria. *Plant Physiol.* **182**, 507-517 (2020).

11. Bassham, J. A., Shibata, K., Steenberg, K., Bourdon, J. and Calvin, M. The photosynthetic cycle and respiration: Light-dark transients. *J. Am. Chem. Soc.* **78**, 4120-4124 (1956).

12. Stitt, M., Wirtz, W. & Heldt, H. W. Metabolite levels during induction in the chloroplast and extrachloroplast compartments of spinach protoplasts. *Biochim. Biophys. Acta.* **593**, 85-102 (1980).

13. Leegood, R. C. & Furbank, R. T. Carbon metabolism and gas exchange in leaves of Zea mays L.: Changes in CO2 fixation, chlorophyll a fluorescence and metabolite levels during photosynthetic induction. *Planta.* **162**, 450-456 (1984).

14. Usuda, H. Changes in Levels of Intermediates of the C(4) Cycle and Reductive Pentose Phosphate Pathway during Induction of Photosynthesis in Maize Leaves. *Plant Physiol.* **78**, 859-864 (1985).

15. Kobza, J. & Edwards, G. E. The photosynthetic induction response in wheat leaves: net CO2 uptake, enzyme activation, and leaf metabolites. *Planta* **171**, 549-559 (1987).

16. Janasch, M., Asplund-Samuelsson, J., Steuer, R. & Hudson, E. P. Kinetic modeling of the Calvin cycle identifies flux control and stable metabolomes in *Synechocystis* carbon fixation. *J. Exp. Bot.* **70**, 973-983 (2019).

17. Ponce-Toledo, R. I. et al. An Early-Branching Freshwater Cyanobacterium at the Origin of Plastids. *Curr. Biol.* **27**, 386-391 (2017).

18. Shimizu, H. & Toya, Y. Recent advances in metabolic engineering-integration of in silico design and experimental analysis of metabolic pathways. *J. Biosci. Bioeng.* **132**, 429-436 (2021).

19. Sauer, U. Metabolic networks in motion: 13C-based flux analysis. *Mol. Syst. Biol.* **2**, 62 (2006).

20. Leighty, R. W. & Antoniewicz, M. R. Dynamic metabolic flux analysis (DMFA): a framework for determining fluxes at metabolic non-steady state. *Metab. Eng.* **13**, 745-755 (2011).

21. Niklas, J., Schräder, E., Sandig, V., Noll, T. & Heinzle, E. Quantitative characterization of metabolism and metabolic shifts during growth of the new human cell line AGE1.HN using time resolved metabolic flux analysis. *Bioprocess Biosyst. Eng.* **34**, 533-545 (2011).

22. Vallino, J. J. & Stephanopoulos, G. Metabolic flux distributions in *Corynebacterium glutamicum* during growth and lysine overproduction. *Biotechnol. Bioeng.* **41**, 633-646

(1993).

23. Pinu, F. R., Villas-Boas, S. G. & Aggio, R. Analysis of Intracellular Metabolites from Microorganisms: Quenching and Extraction Protocols. *Metabolites.* **7**, E53 (2017).

24. Rabinowitz, J. D. & Kimball, E. Acidic acetonitrile for cellular metabolome extraction from Escherichia coli. *Anal. Chem.* **79**, 6167-6173 (2007).

25. Annesley, T. M. Ion suppression in mass spectrometry. *Clin. Chem.* **49**, 1041-1044 (2003).

26. Tanaka, K. et al. Quantification of NAD(P)H in cyanobacterial cells by a phenol extraction method. *Photosynth. Res.* **148**, 57-66 (2021).

27. Shimakawa, G. et al. FLAVODIIRON2 and FLAVODIIRON4 proteins mediate an oxygen-dependent alternative electron flow in *Synechocystis* sp. PCC 6803 under CO_2-limited conditions. *Plant. Physiol.* **167**, 472-480 (2015).

28. Wu, L. et al. Quantitative analysis of the microbial metabolome by isotope dilution mass spectrometry using uniformly 13C-labeled cell extracts as internal standards. *Anal. Biochem.* **336**, 164-171 (2005).

29. Bennett, B. D. et al. Absolute metabolite concentrations and implied enzyme active site occupancy in *Escherichia coli*. *Nat. Chem. Biol.* **5**, 593-599 (2009).

30. Dempo, Y., Ohta, E., Nakayama, Y., Bamba, T. & Fukusaki, E. Molar-based targeted metabolic profiling of cyanobacterial strains with potential for biological production. *Metabolites.* **4**, 499-516 (2014).

31. Nishino, S., Okahashi, N., Matsuda, F. & Shimizu, H. Absolute quantitation of glycolytic intermediates reveals thermodynamic shifts in *Saccharomyces cerevisiae* strains lacking *PFK1* or *ZWF1* genes. *J. Biosci. Bioeng.* **120**, 280-286 (2015).

32. Kauny, J. & Sétif, P. NADPH fluorescence in the cyanobacterium *Synechocystis* sp. PCC 6803: a versatile probe for in vivo measurements of rates, yields and pools. *Biochim. Biophys. Acta.* **1837**, 792-801 (2014).

33. Yoo, S. H., Lee, B. H., Moon, Y., Spalding, M. H. & Jane, J. L. Glycogen synthase isoforms in *Synechocystis* sp. PCC6803: identification of different roles to produce glycogen by targeted mutagenesis. *PLoS One.* **9**, e91524 (2014).

34. Hasunuma, T., Matsuda, M., Kato, Y., Vavricka, C. J. & Kondo, A. Temperature enhanced succinate production concurrent with increased central metabolism turnover in the cyanobacterium *Synechocystis* sp. PCC 6803. *Metab. Eng.* **48**, 109-120 (2018).

35. Tamoi, M., Takeda, T. & Shigeoka, S. Functional analysis of Fructose-1,6-bisphosphatase isozymes (*fbp-I* and *fbp-II* gene products) in cyanobacteria. *Plant Cell Physiol.* **40**, 257-261 (1999).

36. Miller, A. G. & Canvin, D. T. Glycolaldehyde Inhibits CO_2 Fixation in the Cyanobacterium *Synechococcus* UTEX 625 without Inhibiting the Accumulation of

578 Inorganic Carbon or the Associated Quenching of Chlorophyll *a* Fluorescence. *Plant.*
579 *Physiol.* **91**, 1044-1049 (1989).
580 37. Tsukamoto, Y., Fukushima, Y., Hara, S. & Hisabori, T. Redox control of the activity of
581 phosphoglycerate kinase in *Synechocystis* sp. PCC6803. *Plant Cell. Physiol.* **54**, 484-491
582 (2013).
583 38. McFarlane, C. R. et al. Structural basis of light-induced redox regulation in the
584 Calvin-Benson cycle in cyanobacteria. *Proc. Natl. Acad. Sci. USA.* **116**, 20984-20990
585 (2019).
586 39. Feng, L. et al. Structural and biochemical characterization of
587 fructose-1,6/sedoheptulose-1,7-bisphosphatase from the cyanobacterium *Synechocystis*
588 strain 6803. *FEBS J.* **281**, 916-926 (2014).
589 40. Mallén-Ponce, M. J., Huertas, M. J., Sánchez-Riego, A. M. & Florencio, F. J. Depletion of
590 m-type thioredoxin impairs photosynthesis, carbon fixation, and oxidative stress in
591 cyanobacteria. *Plant Physiol.* **187**, 1325-1340 (2021).
592 41. Liang, F. & Lindblad, P. Effects of overexpressing photosynthetic carbon flux control
593 enzymes in the cyanobacterium *Synechocystis* PCC 6803. *Metab. Eng.* **38**, 56-64 (2016).
594 42. Marcus, Y. & Gurevitz, M. Activation of cyanobacterial RuBP-carboxylase/oxygenase is
595 facilitated by inorganic phosphate via two independent mechanisms. *Eur. J. Biochem.* **267**,
596 5995-6003 (2000).
597 43. Perchorowicz, J. T., Raynes, D. A. & Jensen, R. G. Light limitation of photosynthesis and
598 activation of ribulose bisphosphate carboxylase in wheat seedlings. *Proc. Natl. Acad. Sci.*
599 *USA.* **78**, 2985-2989 (1981).
600 44. Seemann, J. R., Kirschbaum, M. U., Sharkey, T. D. & Pearcy, R. W. Regulation of
601 Ribulose-1,5-Bisphosphate Carboxylase Activity in *Alocasia macrorrhiza* in Response to
602 Step Changes in Irradiance. *Plant Physiol.* **88**, 148-152 (1988).
603 45. Ito, S. & Osanai, T. Unconventional biochemical regulation of the oxidative pentose
604 phosphate pathway in the model cyanobacterium *Synechocystis* sp. PCC 6803. *Biochem.*
605 *J.* **477**, 1309-1321 (2020).
606 46. Christodoulou, D. et al. Reserve Flux Capacity in the Pentose Phosphate Pathway Enables
607 *Escherichia coli*'s Rapid Response to Oxidative Stress. *Cell Syst.* **6**, 569-578.e7 (2018).
608 47. Maruyama, M. et al. Time-resolved analysis of short term metabolic adaptation at dark
609 transition in *Synechocystis* sp. PCC 6803. *J. Biosci. Bioeng.* **128**, 424-428 (2019).
610 48. Gleizer, S. et al. Conversion of Escherichia coli to Generate All Biomass Carbon from
611 CO2. *Cell.* **179**, 1255-1263.e12 (2019).
612 49. Gassler, T. et al. The industrial yeast Pichia pastoris is converted from a heterotroph into
613 an autotroph capable of growth on CO2. *Nat. Biotechnol.* **38**, 210-216 (2020).

50. Williams, J. G. K. Construction of specific mutations in photosystem II photosynthetic reaction center by genetic engineering methods in *Synechocystis* 6803. *Methods Enzymol.* **167**, 766-778 (1988).

51. Hasunuma, T. et al. Dynamic metabolic profiling of cyanobacterial glycogen biosynthesis under conditions of nitrate depletion. *J. Exp. Bot.* **64**, 2943-2954 (2013).

Acknowledgements

This work was supported by the Mirai Program [grant number JPMJMI19E4] from the Japan Science and Technology Agency (JST) of the Ministry of Education, Culture, Sports, Science, and Technology (MEXT), Japan, and the Japan Society for the Promotion of Science (JSPS) Kakenhi (Grants-in-Aid for Scientific Research) Grant Number 21J00113.

Author contributions

K.T. and T.H. designed the research. K.T. and M.M. performed research. K.T. and T.S. analyzed data. K.T., T.S., A.K. and T.H. wrote the article.

Competing interests

The authors declare no competing interests.

633 **Figures**

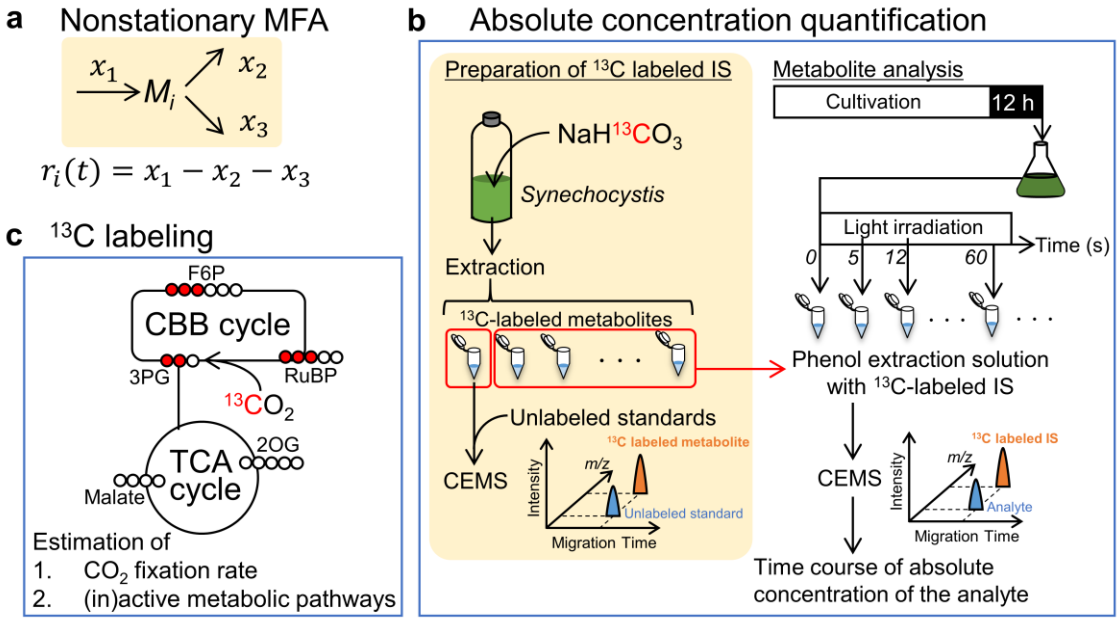

634

635 **Fig. 1 Process for estimating temporal changes in metabolic flux. a,** Relationship between
636 concentration change and metabolic flux. r_i(t) is the accumulation rate of metabolite M_i. x_n represents
637 metabolic flux of the *n*th reaction. **b,** Experimental procedure for quantifying absolute metabolite
638 concentration. **c,** Schematic example of isotope-labeled state during $^{13}CO_2$ incorporation. Empty and
639 red-filled circles represent unlabeled and labeled carbon atoms, respectively. Abbreviations: CBB,
640 Calvin-Benson-Bassham; CEMS, capillary electrophoresis-mass spectrometry; F6P, fructose
641 6-phosphate; IS, internal standard; RuBP, ribulose 1,5-bisphosphate; TCA, tricarboxylic acid; 2OG,
642 2-oxoglutarate; 3PG, 3-phosphoglycerate.

643

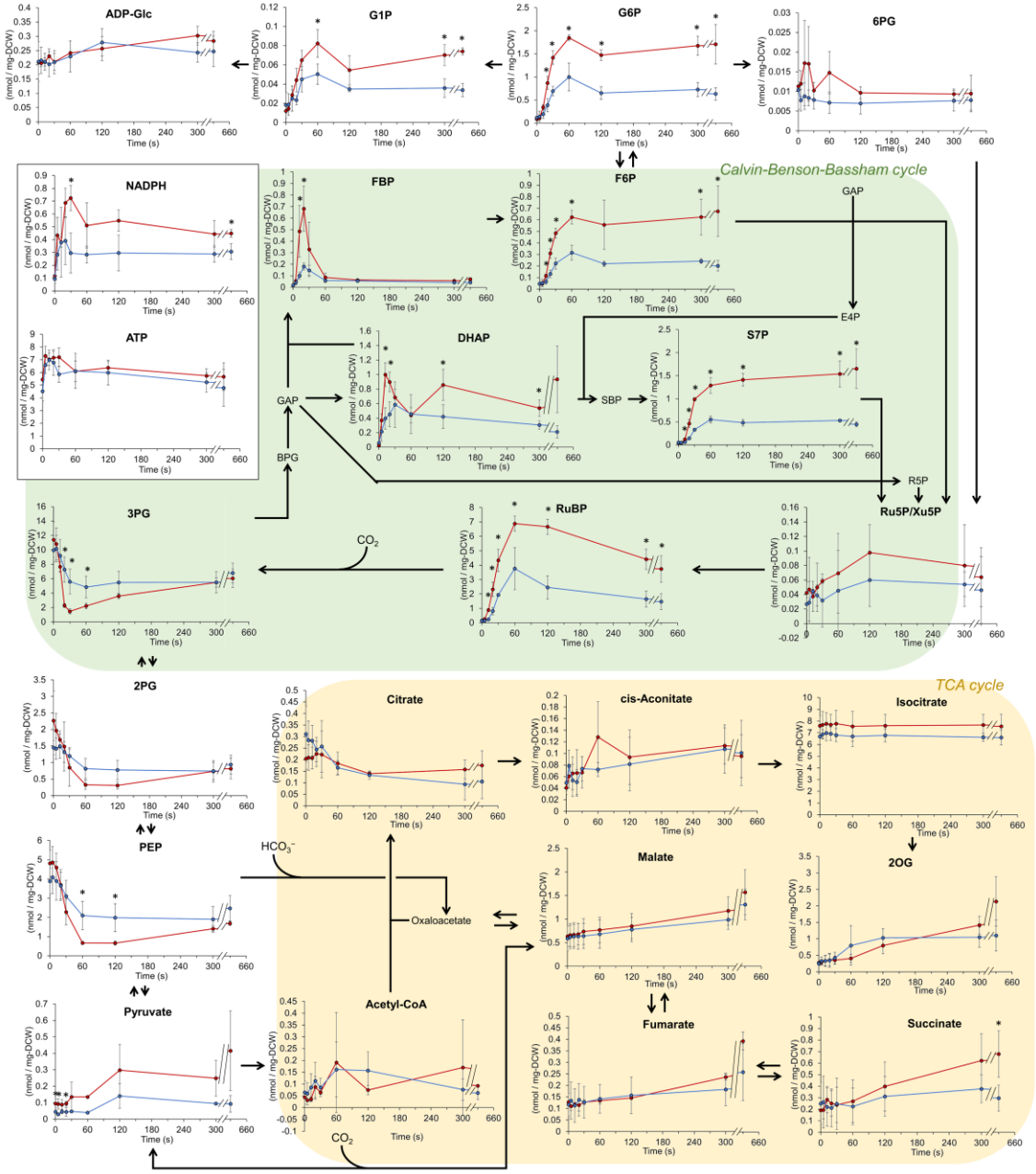

Fig. 2 Rapid temporal change of absolute metabolite concentration during photosynthesis start. Intracellular metabolites were extracted at the indicated times after transition from darkness to light-irradiated condition at the intensity of 200 μmol m^{-2} s^{-1} (red line) or 30 μmol m^{-2} s^{-1} (blue line). Levels of glyceraldehyde 3-phosphate (GAP), erythrose 4-phosphate (E4P), and ribose 5-phosphate (R5P) were below the detection limit (0.001 nmol / mg DCW). 1,3-Bisphosphoglycerate (BPG) and sedoheptulose 1,7-bisphosphate (SBP) were not identified due to lack of commercial reagent for use as a standard. Black arrows indicate metabolic pathways. Abbreviations: DCW, dry cell weight; DHAP, dihydroxyacetonephosphate; FBP, fructose 1,6-bisphosphate; F6P, fructose 6-phosphate; G1P, glucose 1-phosphate; G6P, glucose 6-phosphate;

2OG, 2-oxoglutarate; PEP, phosphoenolpyruvate; 6PG, 6-phosphogluconate; 2PG, 2-phosphoglycerate; 3PG, 3-phosphoglycerate; RuBP, ribulose 1,5-bisphosphate; Ru5P, ribulose 5-phosphate; S7P, sedoheptulose 7-phosphate; Xu5P, Xylulose 5-phosphate. Values are mean ± SD (bars) of three independent experiments. Significant differences between the two light intensities were evaluated by a two-tailed non-paired Student's t test (* $p < 0.05$).

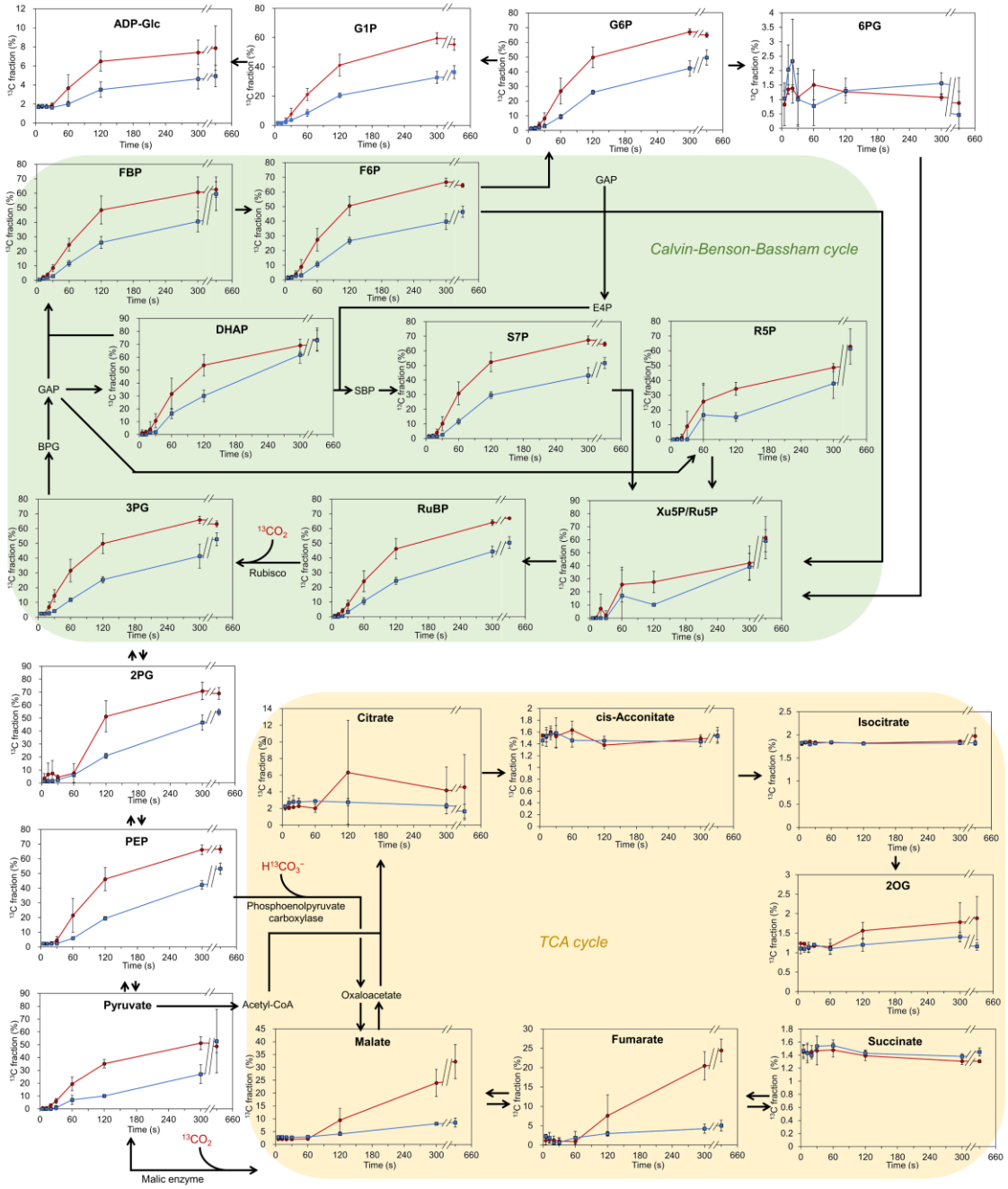

Fig. 3 Time course of ^{13}C fraction of metabolites following light irradiation at 200 µmol m^{-2} s^{-1} (red line) or 30 µmol m^{-2} s^{-1} (blue line). Values are mean ± SD (bars) of three biological replicates. Black arrows indicate metabolic pathways. Abbreviations are as in Figure 2 legend.

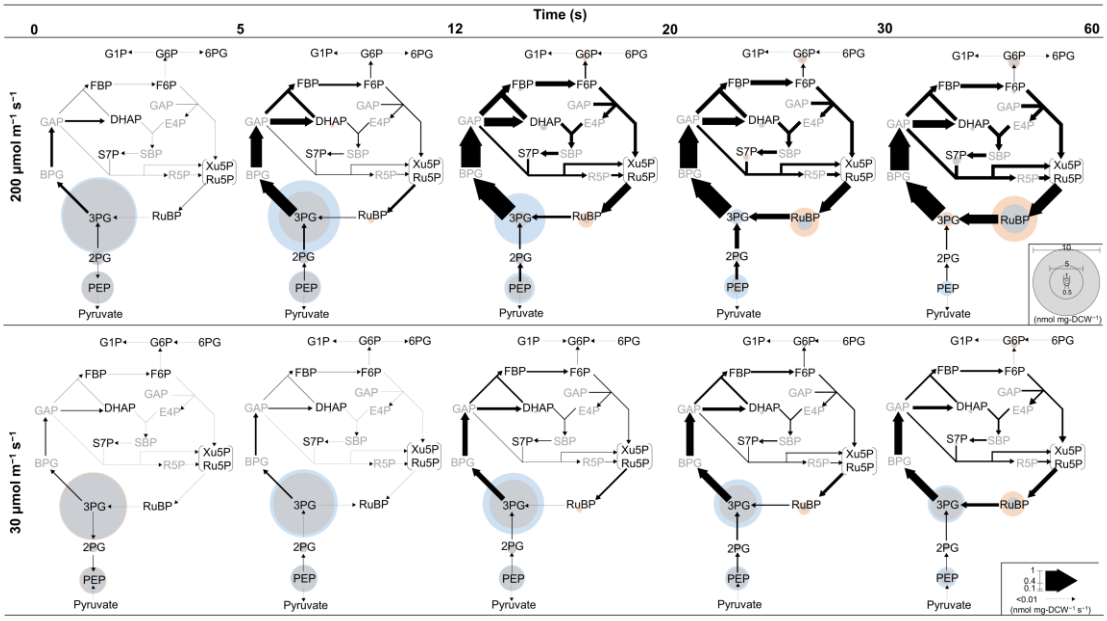

Fig. 4 Estimated change in metabolic flux after initiating light irradiation at 200 μmol m^{-2} s^{-1} (upper row) and 30 μmol m^{-2} s^{-1} (lower row). Metabolic fluxes are indicated as thickness of arrows with the values in the scale bar in the lower right corner. Metabolite concentrations at the beginning and end of each time interval are indicated by diameters of blue and orange circles, respectively. Overlap between orange and blue circles (namely invariant concentration during a time interval) is shown in gray. Abbreviations are as in Figure 2 legend.

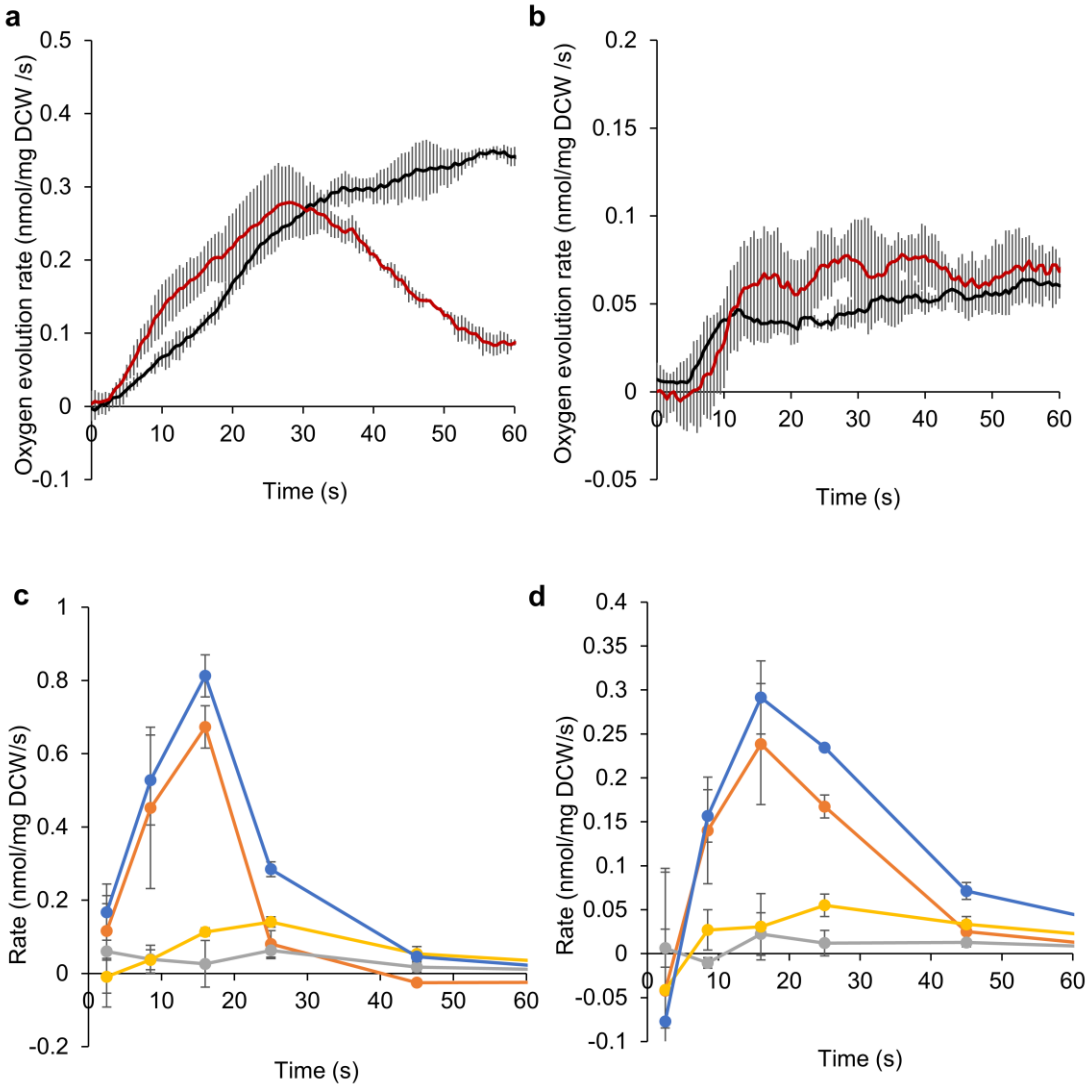

Fig. 5 Oxygen evolution rate in the presence of glycolaldehyde (GA) and comparison with metabolite variation rate. a, b, Oxygen evolution rate in the absence (black line) and presence (red line) of GA after light irradiation at the intensity of 200 μmol m^{-2} s^{-1} (**a**) or 30 μmol m^{-2} s^{-1} (**b**). GA (10 mM) was added before the initiation of light irradiation. **c, d,** Decreasing rate of 3PG (orange line), PEP (yellow line), and 2PG (gray line), and the sum of these three metabolites (blue line) after initiation of light irradiation at the intensity of 200 μmol m^{-2} s^{-1} (**c**) or 30 μmol m^{-2} s^{-1} (**d**). Since the decreasing rates were derived from two consecutive concentration data points, values are plotted at a time point representing the average (mean) of the two time points. For all panels, values are plotted as mean ± SD (bars) of three biological replicates. Abbreviations are as in Figure 2 legend.

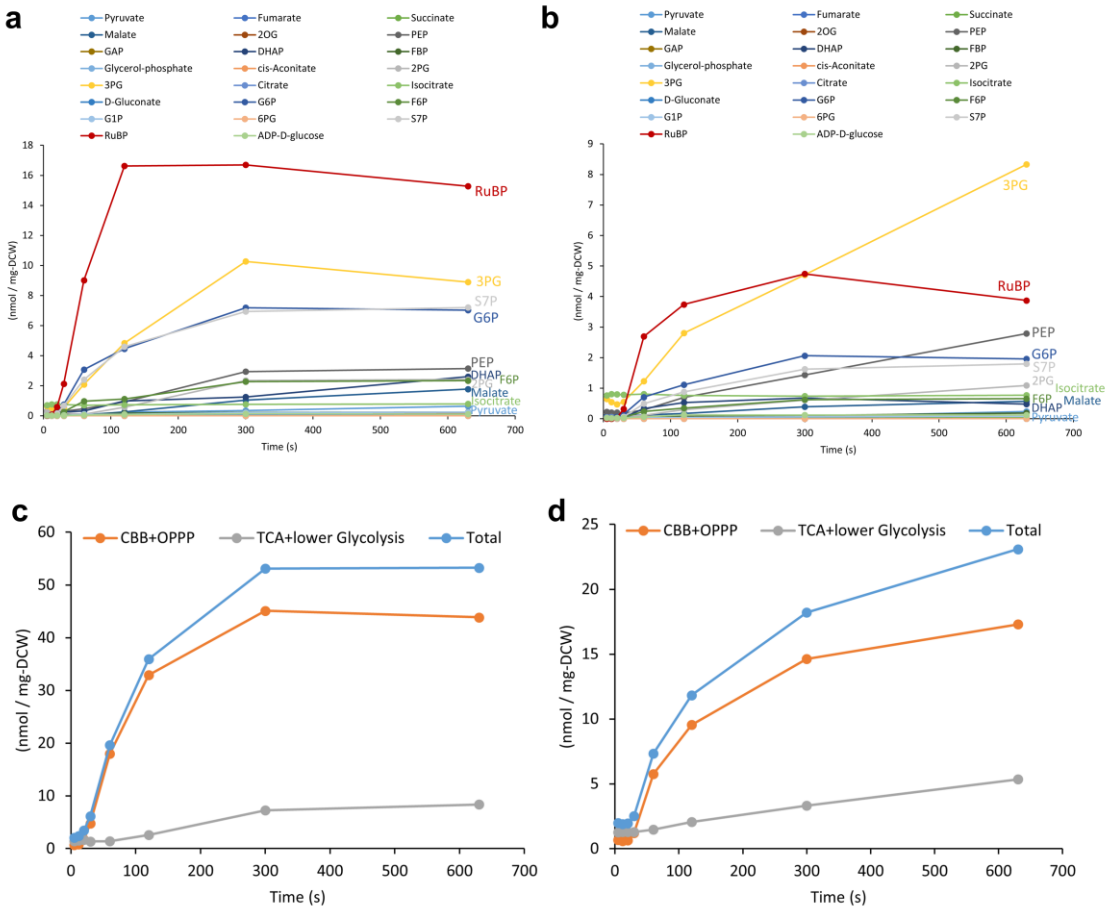

686

687 **Extended Data Fig. 1 Time course of ^{13}C level in each metabolite (a, b) and total ^{13}C level (c, d).**
688 Number of ^{13}C atoms was calculated as mean of ^{13}C enrichment multiplied by mean metabolite
689 concentration and the number of C atoms in the molecule for the two light intensities: (a, c) 200
690 μmol m^{-2} s^{-1}, (b, d) 30 μmol m^{-2} s^{-1}. (c, d) Number of ^{13}C atoms was summed for CBB cycle and
691 oxidative pentose phosphate pathway (OPPP) intermediates (orange line), TCA cycle, and glycolysis
692 intermediates (gray line), and all measured metabolites (blue line). Abbreviations are as in Figure 2
693 legend.
694

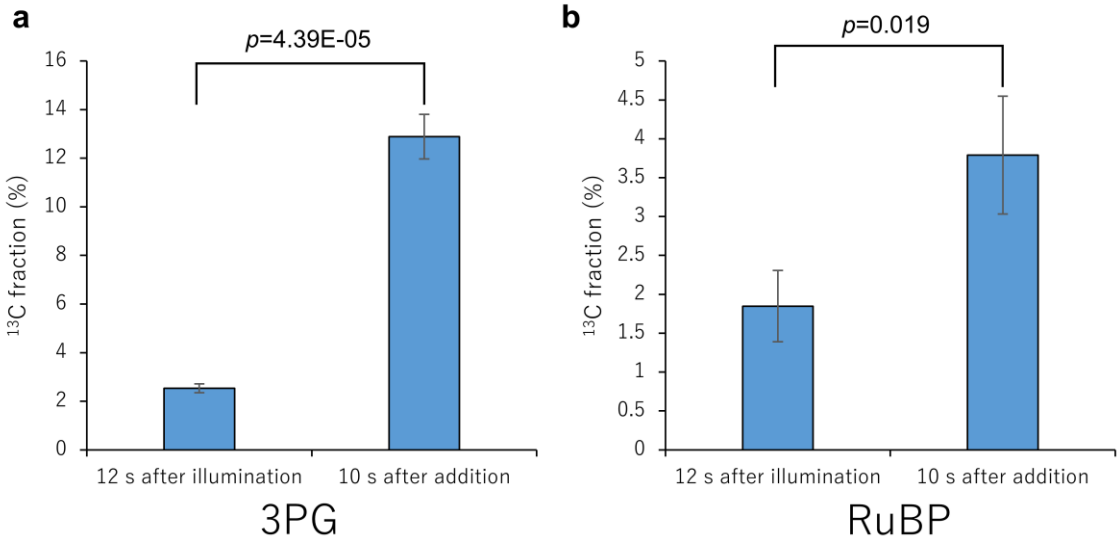

Extended Data Fig. 2 Effect of pre-illumination on the start of ^{13}C incorporation. ^{13}C fractions of (a) 3-phosphoglycerate (3PG) and (b) Ribulose 1,5-bisphosphate (RuBP) after 12 s of illumination (200 μmol m^{-2} s^{-1}) of the 12-h dark-adapted cells were lower than those at 10 s after addition of 1 mM $NaH^{13}CO_3$ to cells that had been pre-illuminated (200 μmol m^{-2} s^{-1}) for 5 min. Presumably, the higher ^{13}C incorporation rate in pre-illuminated cells reflects the fact that CO_2 fixation already had been activated (by pre-illumination) prior to the addition of $NaH^{13}CO_3$. Thus, lower ^{13}C incorporation by dark-adapted cells can be attributed to the low activation state of CO_2 fixation during photosynthetic induction. Values are mean ± SD (bars) of three biological replicates. Significant differences were evaluated by a two-tailed non-paired Student's t test; *p* values were as indicated.

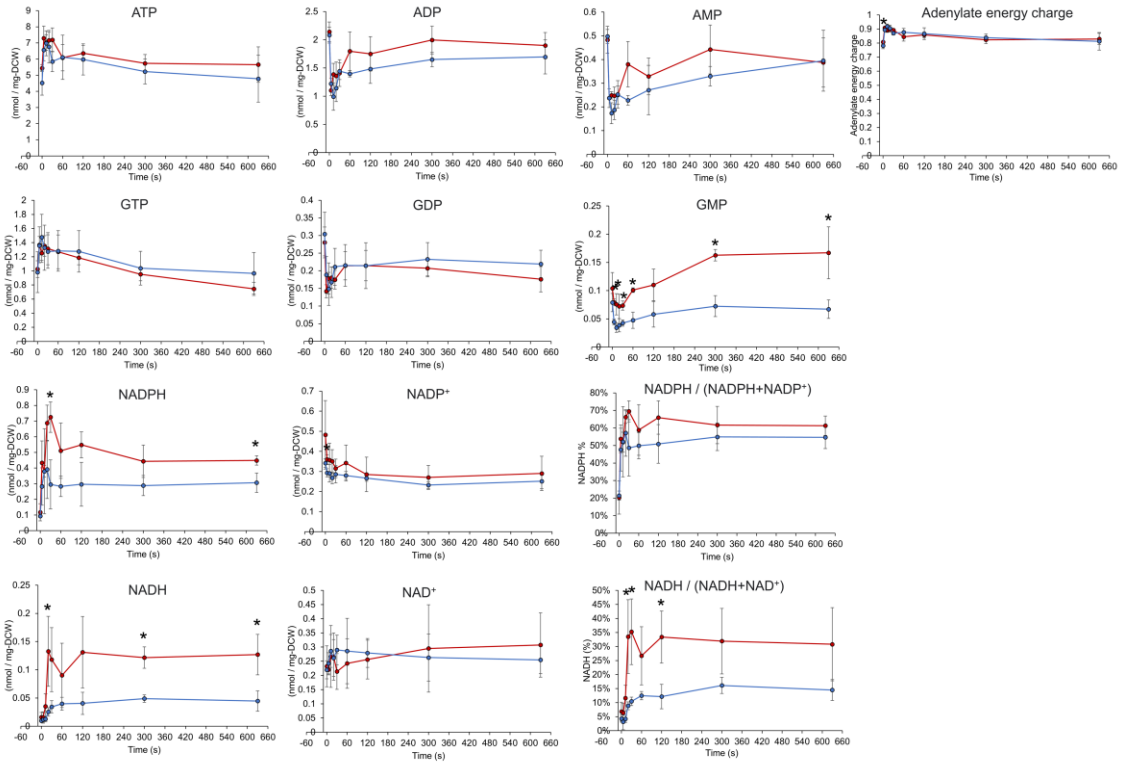

Extended Data Fig. 3 Concentration transients of cofactors during photosynthetic induction. Intracellular metabolites were extracted at the indicated times after transition from darkness to light-irradiated conditions at the intensity of 200 μmol m^{-2} s^{-1} (red line) or 30 μmol m^{-2} s^{-1} (blue line). Values are mean ± SD (bars) of three independent experiments. Significant differences between the two light intensities were evaluated by a two-tailed non-paired Student's t test (* $p < 0.05$). Abbreviations: ADP, Adenosine diphosphate; AMP, adenosine monophosphate; ATP, adenosine triphosphate; GDP, Guanosine diphosphate; GMP, Guanosine monophosphate; GTP, Guanosine triphosphate; NAD(P), nicotinamide adenine dinucleotide (phosphate)

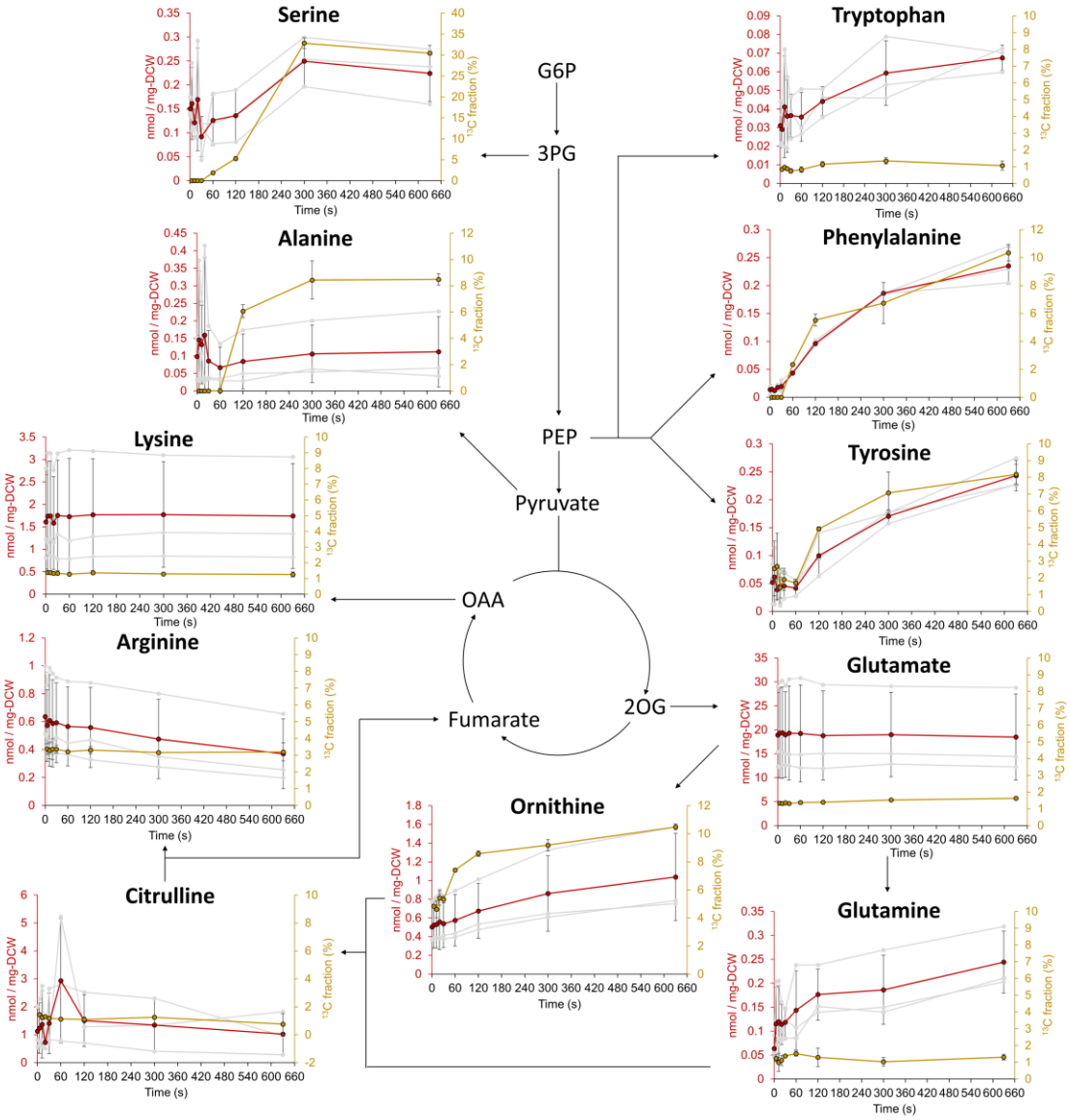

Extended Data Fig. 4 Concentration and ^{13}C fraction transients of amino acids during photosynthetic induction of cells illuminated at the intensity of 200 μmol m^{-2} s^{-1}. Intracellular metabolites were extracted at the indicated times after transition from darkness to light-irradiated conditions at the intensity of 200 μmol m^{-2} s^{-1}. Red lines and yellow lines indicate metabolite concentration and ^{13}C fraction, respectively. Simplified central metabolic pathways are indicated by arrows. Values of concentrations and ^{13}C fractions are mean ± SD (bars) of three and two independent experiments, respectively. Values of metabolite concentrations for individual experiments are indicated by gray lines. Abbreviations are as in Figure 2 legend.

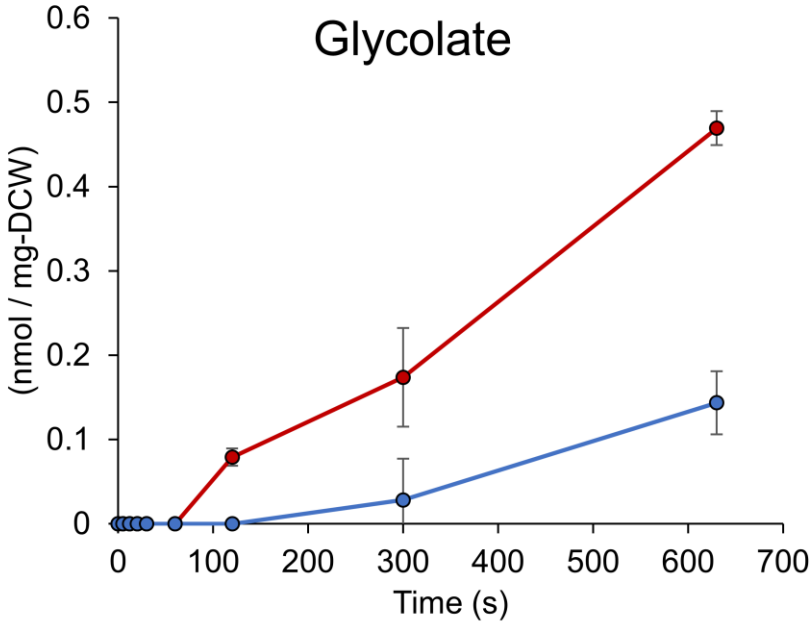

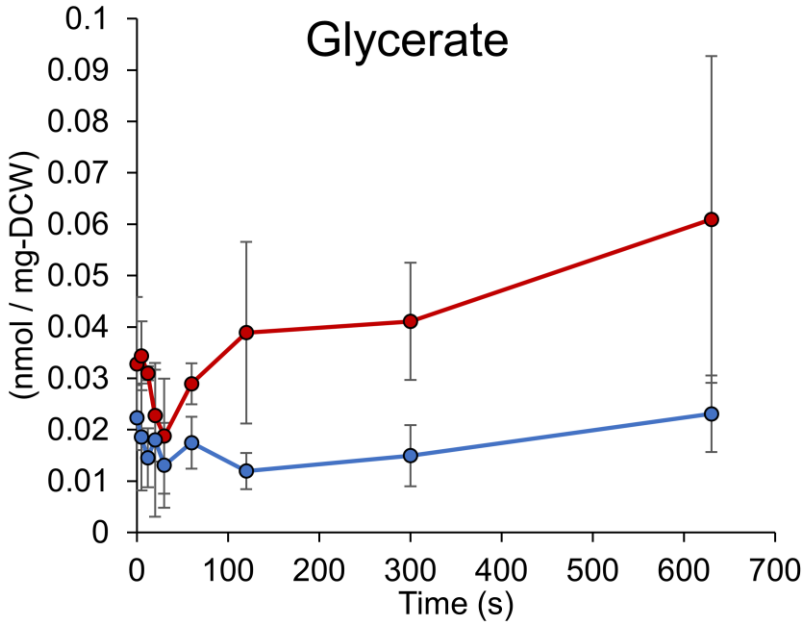

Extended Data Fig. 5 Concentration transients of intermediates in photorespiration pathway during photosynthetic induction. Intracellular metabolites were extracted at the indicated time after transition from darkness to light-irradiated conditions at the intensity of 200 μmol m^{-2} s^{-1} (red line) or 30 μmol m^{-2} s^{-1} (blue line). Values are mean ± SD (bars) of three independent experiments. DCW, dry cell weight

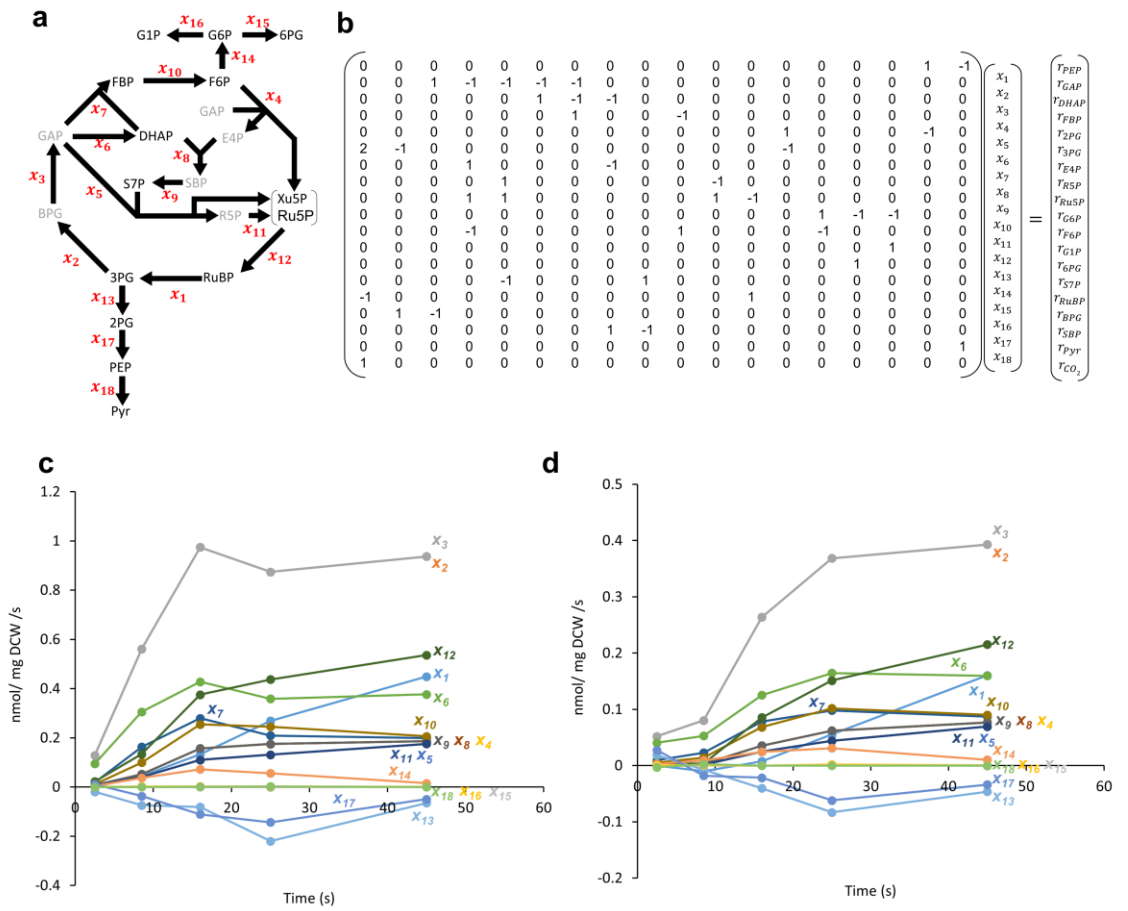

Extended Data Fig. 6 Short-term dynamic metabolic flux analysis (STD-MFA). (a) Metabolic pathways incorporated into calculation for STD-MFA. The experimental data of absolute concentration and ^{13}C incorporation change allowed us to simplify the metabolic model during photosynthetic induction. x_i represents net flux of *i*th metabolic pathway. (b) Detailed form of the mass balance equation used for STD-MFA. For more details, see Methods section. (c, d) Transients of estimated metabolic fluxes during photosynthetic induction in illuminated conditions at (c) 200 μmol m^{-2} s^{-1} or (d) 30 μmol m^{-2} s^{-1}. Since the fluxes were estimated using metabolite accumulation rates derived from two consecutive concentration data points, flux values are plotted at a time point corresponding to the average (mean) of the two time points. Abbreviations are as in Figure 2 legend.

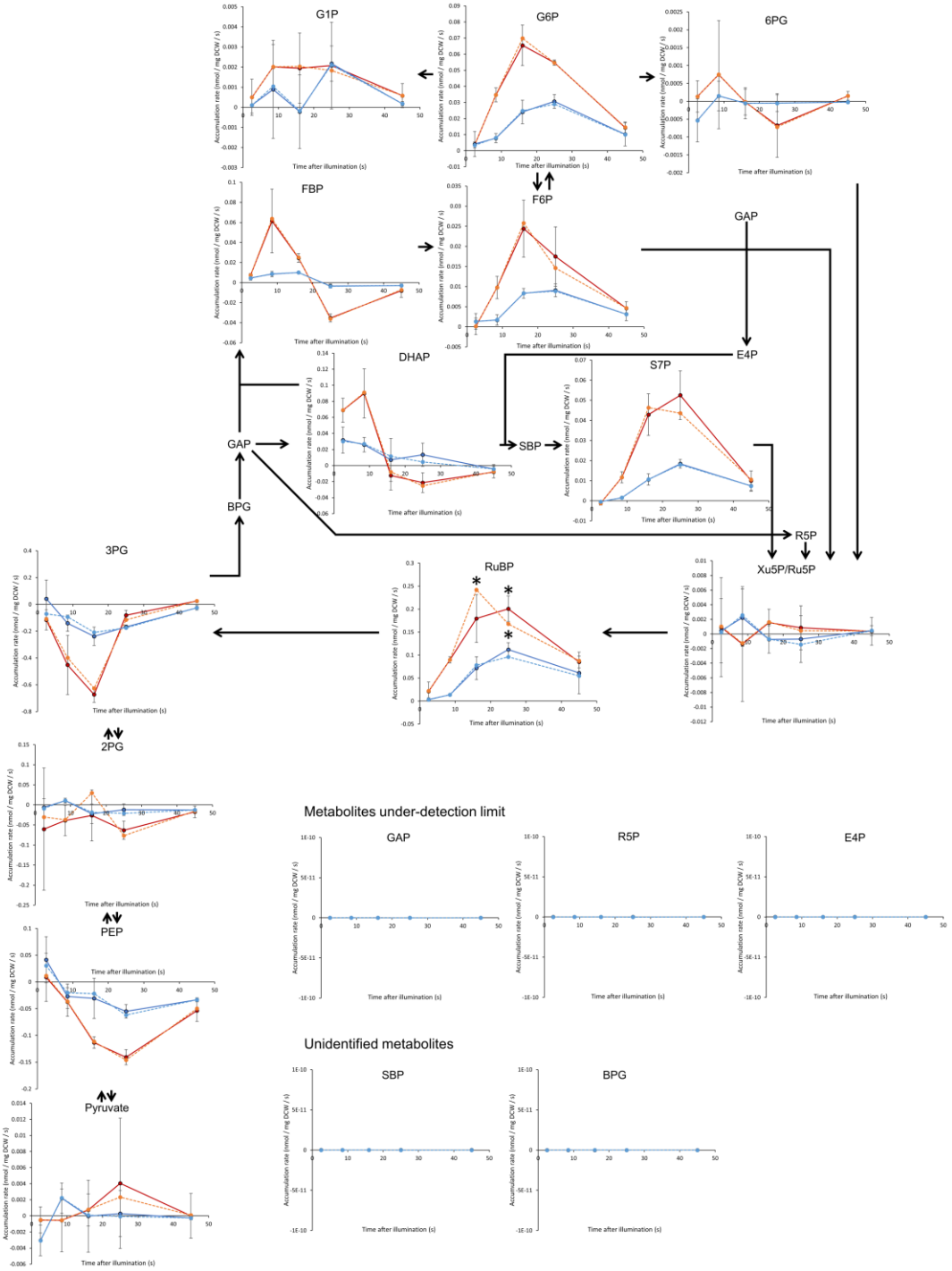

Extended Data Fig. 7 Measured and estimated metabolic accumulation rates. Measured accumulation rates at the light intensity of 200 μmol m^{-2} s^{-1} (red solid line) or 30 μmol m^{-2} s^{-1} (blue solid line) were derived from slope between two consecutive concentration data points shown in Fig. 2. Estimated accumulation rates at the light intensity of 200 μmol m^{-2} s^{-1} (orange dotted line) or 30 μmol m^{-2} s^{-1} (blue dotted line) are shown for validation of the short-term dynamic metabolic flux analysis (STD-MFA) result. Black arrows indicate metabolic pathways. Abbreviations are as in

Figure 2 legend. Values are plotted at the average (mean) time point of the two time points used for the concentration data points. Values of measured accumulation rates are mean ± SD (bars) of three independent experiments. Asterisk indicates that estimated value is out of range of the measured mean ± SD.

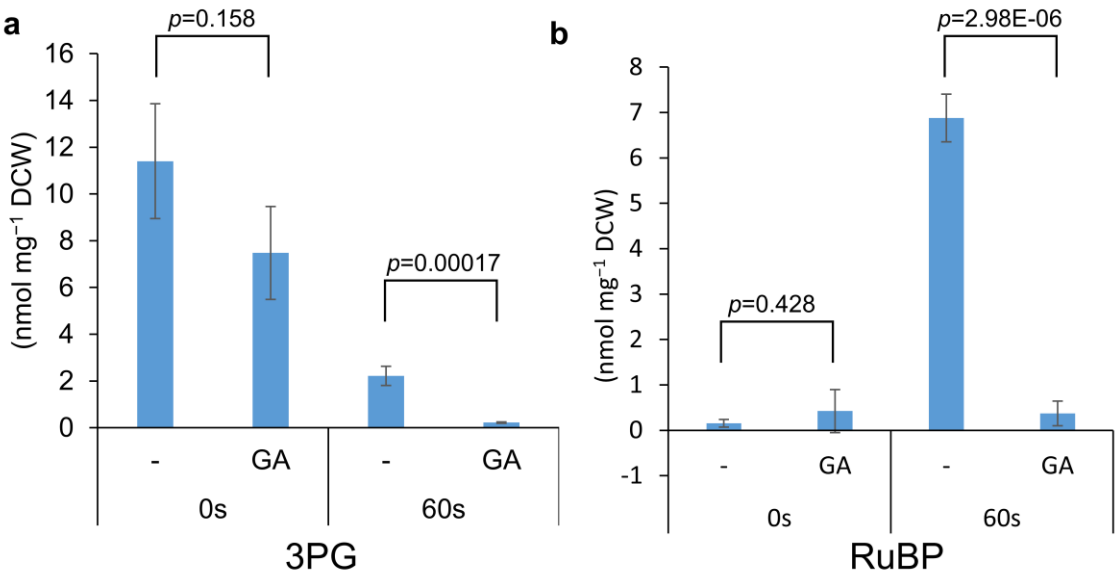

Extended Data Fig. 8 Effect of CBB cycle inhibitor glycolaldehyde (GA) on metabolite concentrations. Absolute concentrations of (a) 3-phosphoglycerate (3PG) and (b) Ribulose 1,5-bisphosphate (RuBP) before light illumination (dark condition; "0 s") and at 60 s after light illumination at 200 μmol m^{-2} s^{-1} were analyzed in the absence (-) and presence (GA) of 10 mM GA. Values are mean ± SD (bars) of three independent experiments. Significant differences were evaluated by a two-tailed non-paired Student's t test, and *p* values were as indicated.

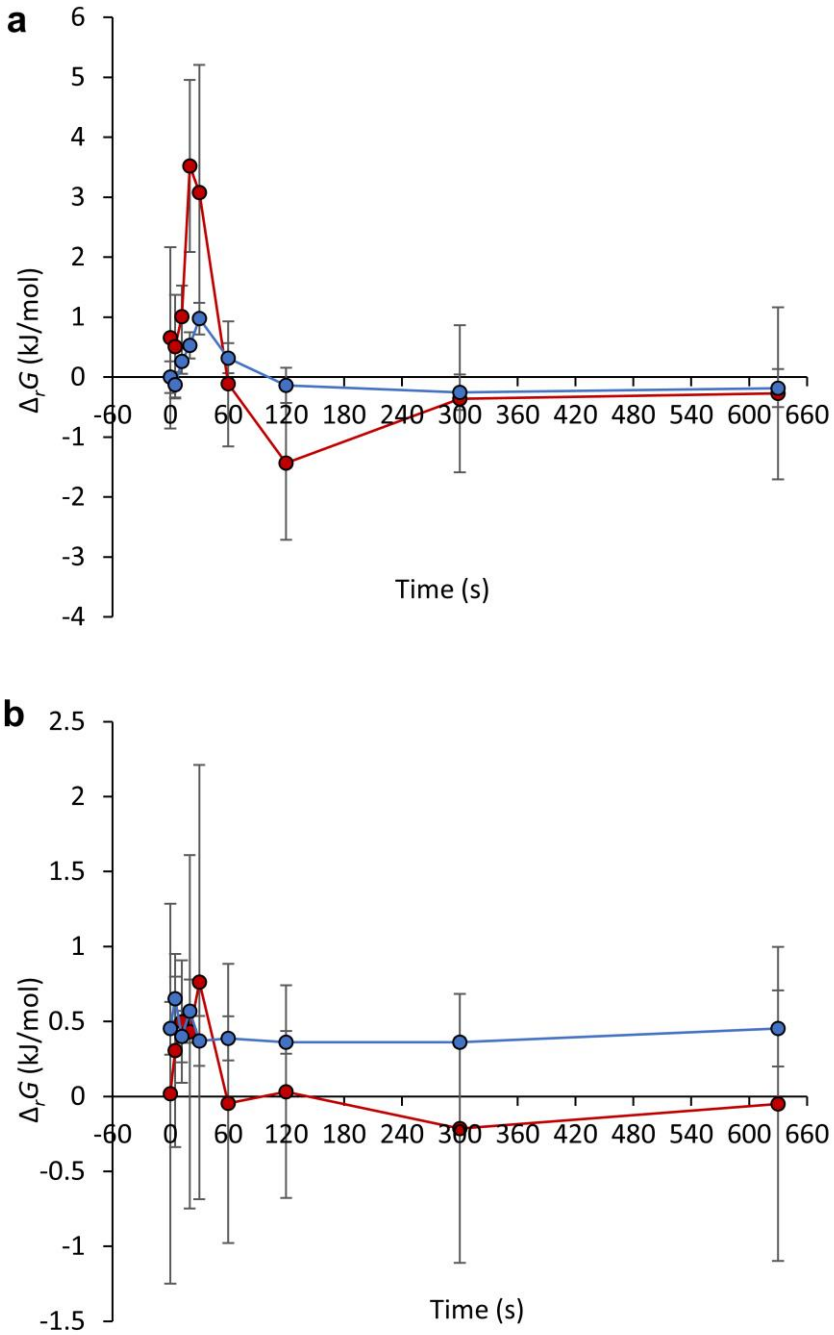

Extended Data Fig. 9 Time course of reaction Gibbs free energy change ($\Delta_r G$). $\Delta_r G$ values of reactions (a) from 3-phosphoglycerate (3PG) to 2-phosphoglycerate (2PG) and (b) from 2PG to phosphoenolpyruvate (PEP) were derived based on equation (2). Red and blue lines indicate $\Delta_r G$ at the illuminated light intensity of 200 μmol m^{-2} s^{-1} and 30 μmol m^{-2} s^{-1}, respectively. Values are mean ± SD (bars) derived from three independent experiments.